

Tailoring gas-phase CO₂ electroreduction selectivity to hydrocarbons at Cu nanoparticles

I Merino-Garcia, J Albo and A Irabien

Department of Chemical and Biomolecular Engineering, University of Cantabria, Avenida de los Castros s/n, 39005, Santander, Cantabria, Spain.

E-mail: merinoi@unican.es

Abstract. Copper-based surfaces appear as the most active catalysts for CO₂ electroreduction to hydrocarbons, even though formation rates and efficiencies still need to be improved. The aim of the present work is to evaluate the continuous gas-phase CO₂ electroreduction to hydrocarbons (i.e. ethylene and methane) at copper nanoparticulated-based surfaces, paying attention to particle size influence (ranging from 25 nm to 80 nm) on reaction productivity, selectivity, and Faraday efficiency for CO₂ conversion. The effect of the current density and the presence of a microporous layer within the working electrode are then evaluated. Copper-based gas diffusion electrodes are prepared by airbrushing the catalytic ink onto carbon supports, which are then coupled to a cation exchange membrane (Nafion) in a membrane electrode assembly. The results show that the use of smaller copper nanoparticles (25 nm) leads to a higher ethylene production (1242 $\mu\text{mol m}^{-2}\text{s}^{-1}$) with a remarkable high Faraday efficiency (91.2 %) and, diminishing, at the same time, the competitive hydrogen evolution reaction. This work demonstrates the importance of nanoparticle size on reaction selectivity, which may be of help to design enhanced electrocatalytic materials for CO₂ valorization to hydrocarbons.

Keywords: CO₂ electroreduction, Cu nanoparticles, hydrocarbons, reaction selectivity, ethylene

1. Introduction

The continuous rise of carbon dioxide (CO₂) emissions into the atmosphere led to an increase of 6 ppm in CO₂ concentration between 2015 and 2017 (406.42 ppm) [1]. This represents an unprecedented 2-years record for the National Oceanic and Atmospheric Administration (NOAA), which has been reporting the rate of CO₂ growth since 1960. It is therefore crucial to reduce CO₂ emissions in order to mitigate the negative effects of global warming. In this context, the utilisation of CO₂ represents an attractive alternative to reduce our reliance on fossil fuels for energy and chemical synthesis, helping also to palliate global warming effects [2].

The electrochemical reduction technology is particularly interesting for CO₂ utilisation, since it allows the storage of intermittent renewable energy in the form of chemical bonds [3]. The slow kinetics of the reaction, the high energy requirements and market limitations, among others, are, however, issues that limit the practical application of this technology [4].

Among the different products obtained from the electroreduction of CO₂ (e.g. carbon monoxide, formic acid, alcohols or hydrocarbons) at different conditions [5-7], the formation of hydrocarbons such as ethylene (C₂H₄) or methane (CH₄) is appealing due to their several applications in the chemical industry as raw materials, energy vectors and fuels [3]. The overpotential of these reactions is too large, which makes these processes energetically inefficient [8]. Besides, the limited productivity rates hinder the CO₂-to-hydrocarbons electrochemical reaction, which is mainly associated to the catalytic material applied.

Up to date, only copper (Cu)-based electrocatalysts seem to be able to electroreduce CO₂ to hydrocarbons with modest reaction rates and efficiencies [9], in which controlling the selectivity to hydrocarbons and reducing the overpotential of the reaction are nowadays two of the most scientific challenges [10]. In this sense, several authors have focused their research on evaluating different aspects of Cu-based catalytic materials such as surface structure, morphology and particle size, showing a dramatic influence on reaction performance [10-14]. For instance, Hori et al. [11-12] analysed the effect of Cu facets on hydrocarbons selectivity, demonstrating that Cu (111) facets favoured the formation of CH₄. In contrast, Cu (100) facets were favourable for the production of C₂H₄ at the same conditions, which can be explained as differences in the chemisorption characteristics of the surfaces [10]. This significant dependence of CO₂ reduction selectivity on surface structure may explain the differences in product formations on electrodeposited Cu and Cu film-based electrocatalysts. On the other hand, the morphological effect has also been studied by using polycrystalline Cu and Cu meshes with mesopores of different width and depth at the nanometre scale [13]. As narrowing and decreasing the pore width and depth the Faraday efficiency (*FE*) to CH₄ significantly decreased. As a consequence, the *FE* to C₂-products (i.e. C₂H₄ and C₂H₆) was enhanced at these conditions. As summary, both local pH and mass flow can be affected by morphology, enhancing C-C coupling reaction and extending retention times of key reaction intermediates. Furthermore, particle size analyses have been carried out for different electrocatalytic reactions such as the oxygen reduction reaction [15] and the electrocatalytic CO oxidation [16], among others. The first study on particle size effect for the electrochemical reduction of CO₂ at Cu nanoparticles in a liquid-liquid reactor configuration was developed by Reske and coworkers in 2014 [10]. The product selectivity was evaluated in the size range of 2 nm to 15 nm. The authors suggested that very small particles (< 3 nm) should be avoided for the production of hydrocarbons due to the increase in the strength of the binding of products (i.e. CO) and intermediate species, favouring the formation of H₂ and CO. However, at the intermediate particle size level (i.e. 5 nm to 15 nm) hydrocarbon formation was favoured owing to the weaker CO and H bonding. Accordingly, similar trends were observed using Cu nanoparticles on different supports [14]. The C₂H₄/CH₄ ratio was highly influenced by the particle size. Larger ratios were observed for smaller particles. Nevertheless, the *FE* to CH₄ was slightly improved as increasing the size of the Cu nanoparticles.

Furthermore, different electrochemical reactor configurations have been reported for the conversion of CO₂ [17, 18]. Among them, the use of membrane reactors allow the separation of cathode and anode compartments, involving an easier separation of reduction products and avoiding their re-oxidation [17, 19]. Moreover, mass transfer limitations in the process have led to apply gas diffusion electrodes (GDEs) and membrane electrode assemblies (MEAs), in which the contact and the transport of ionic species are enhanced [20-23], promoting CO₂ transformation into more reduced products such as hydrocarbons. Besides, the introduction of CO₂ directly as gas is an interesting alternative, which allows avoiding issues related to the low solubility of CO₂ in water [9, 24-26].

Overall, the aim of this work is to evaluate the influence of Cu nanoparticle size (ranging from 25 nm to 80 nm) on reaction productivity, selectivity and *FE* for the continuous gas-phase CO₂ electroreduction to hydrocarbons. As far as the authors know this is the first attempt in the literature to evaluate the effect of electrocatalyst size in gas-phase CO₂ electroreduction systems, although the effects of Cu nanoparticle size in the range 2-15 nm on the catalytic electroreduction of CO₂ has been previously evaluated in liquid-phase-based systems [10]. Consequently, this study may contribute to a better understanding of the performance of the process at a larger Cu nanometer size range (25-80 nm). The performance of the Cu-GDE system is tested using a filter-press type electrochemical membrane reactor in continuous operation. The effect of the current density (*j*) applied and the presence of a diffusion

microporous layer (MPL) within the working electrode structure is also analyzed. The obtained results may provide new insights in the development of highly active catalytic materials for CO₂-to-hydrocarbons electrochemical reactions.

2. Experimental details

2.1. Cu-GDE preparation and characterization

Table 1 summarises the main technical features of the electrocatalytic materials evaluated in the present study. Cu nanoparticles (NPs) with different particle size were provided by Sigma-Aldrich. Regarding the manufacturing process of the different GDEs, a Toray paper was used as carbon support (TGP-H-60, Toray Inc.). The catalytic layer was prepared by air-brushing a catalytic ink composed by a mixture of Cu NPs, a Nafion solution (5 wt %, Alfa Aesar, copolymer polytetrafluoroethylene) as binder, and isopropanol (IPA) (AcroSeal, Extra Dry 99.5 % purity) as vehicle, with a 70:30 Cu/Nafion mass ratio and 3 wt% of solids (Cu + Nafion). The final mixture was agitated in an ultrasound bath for at least 30 min. Under these conditions, Cu GDEs with a geometric surface area (*A*) of 10 cm² and a Cu loading (*L*) of 0.5 mgcm⁻² were obtained. The assembly of the membrane (Nafion 117) with the Cu-GDE in a MEA was completed at 323 K and 80 bar using a filter press (Carver, Inc., United States).

Table 1. Electrocatalytic Cu materials applied.

Nomenclature	Size (nm)	Purity (%)
Cu25	25	-
Cu40-60	40-60	>99.5
Cu60-80	60-80	>99.5

The MPL ink includes Vulcan carbon powder (VXC72R, Cabot, carbon black) and polytetrafluoroethylene, PTFE (Sigma-Aldrich, 60 wt% dispersion in H₂O) with a 70:30 Vulcan/PTFE mass ratio. The mixture was then diluted to 3 % in IPA and agitated in an ultrasound bath. This solution was air-brushed onto the Toray paper and the obtained MPL layer was sintered at 623 K for 30 min.

The Cu-based GDEs were electrochemically characterised by cyclic voltammetry (CV) tests in a three-electrode undivided cell, in which a CO₂ saturated-based 0.1 M potassium bicarbonate (KHCO₃) aqueous solution was used as electrolyte. A graphite rod and an Ag/AgCl electrode were used as counter and reference electrodes, respectively. Small pieces of Cu-GDEs (Cu NP= 25 nm, 40-60 nm and 60-80 nm) were used as working electrodes. The resulting *j* were normalised to the geometric area of the electrode. The applied potential was controlled using a MSTAT4 system (Arbin Instruments) and the samples were cycled five times from 0 V vs. Ag/AgCl to -2 V vs. Ag/AgCl.

2.2. CO₂ electroreduction tests

The experimental setup to perform the gas-phase CO₂ electroreduction has been described in our previous study [9]. The core of the filter-press type electrochemical reactor is the MEA, which serves as working electrode and separates the cathode and anode compartments. A dimensionally stable anode [DSA/O₂(Ir-MMO (Mixed Metal Oxide) on Platinum)] and a leak-free Ag/AgCl were used as counter and reference electrodes, respectively. Humidified CO₂ was fed to the cathode compartment at a flow rate, *Q_g/A*, of 18 mLmin⁻¹cm⁻² and a 0.1 M KHCO₃ aqueous solution was used as anolyte. The CO₂ reduction experiments were conducted at galvanostatic conditions (*j*=7.5, 15, 30 mAcm⁻²) using an AutoLab PGSTAT 302N potentiostat. All experiments were carried out at ambient conditions. Gas reduction products were analyzed using a four-channel gas microchromatograph (3000 micro GC, Inficon) equipped with a

thermal conductivity detector (TCD). Gas samples were measured every 5 min for 45 min, with three replicates for each experiment to obtain an averaged reaction rate, r ($\mu\text{molm}^{-2}\text{s}^{-1}$), selectivity, S , defined as the ratio between $r_{\text{C}_2\text{H}_4}$ and r_x , with x being CH_4 and H_2 , and FE , for each product.

3. Results and discussion

3.1. Cyclic voltammetry tests

Figure 1.a. shows the current-voltage responses after 5 electrochemical scans for the Cu NP based-GDEs (i.e. 25 nm, 40-60 nm and 60-80 nm) and that response for the Toray paper for comparison. Additionally, to further analyse the catalytic activity for CO_2 electroreduction, figure 1.b. reveals the CV results for the Cu25-GDE in the absence of CO_2 (under N_2 saturation).

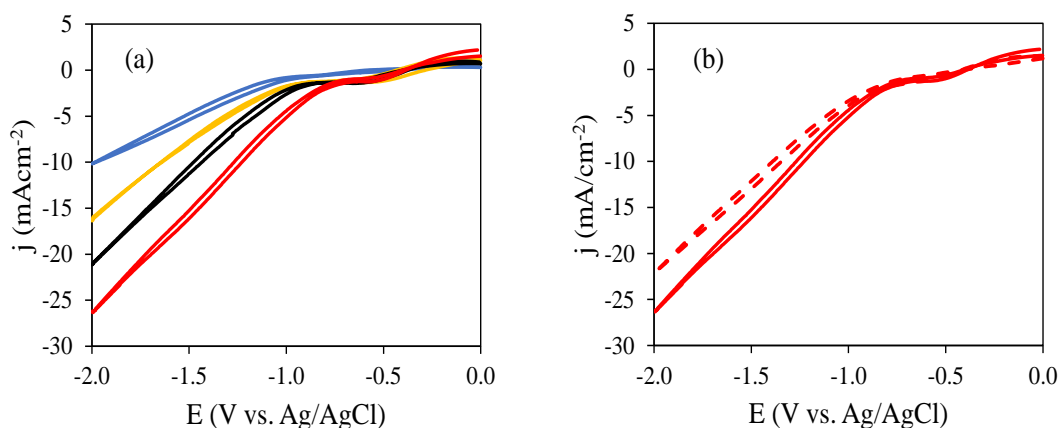


Figure 1. Cyclic voltammograms for: (a) Cu-GDEs in CO_2 -saturated 0.1 M KHCO_3 aqueous electrolyte. Colour codes: Toray paper (blue), Cu25 (red), Cu40-60 (black), Cu60-80 (yellow) and, (b) Cu25-GDE in CO_2 (continuous-red line) and N_2 (dotted-red line) saturated 0.1 M KHCO_3 solution.

Figure 1.a. displays similar trends for all the Cu-based electrodes, even though higher activities can be clearly observed when decreasing Cu nanoparticle size (from 60-80 nm to 25 nm). The main characteristic of the CV voltammograms is the difference between the starting potentials for the reduction process as a function of each material tested, which may be initially associated with the particle size influence on reaction mechanisms [10], involving different pathways and reaction intermediates. For instance, larger Cu particle-based GDEs (i.e. 60-80 and 40-60 nm) presented a similar CO_2 reduction peak (starting at around -0.9 V vs. Ag/AgCl). However, Cu25-based GDEs reached an onset potential of about -0.8 V vs. Ag/AgCl. The highest catalytic activity of the Cu25-based electrode (continuous-red line) might be related to an increase in the fraction of under-coordinated sites, such as defects, edges and corners on the electrode surface due to the smaller size of the Cu NPs, which might involve an increased reaction selectivity to more reduced species [14]. Figure 1.b. demonstrated the reduction of CO_2 molecule, as the activity increased in comparison to that curve under N_2 conditions.

3.2. Gas-phase CO_2 electroreduction

Figure 2 shows the time evolution for the potential (E) and the reaction rate (r) in the continuous gas-phase CO_2 electrochemical conversion to C_2H_4 and CH_4 at the GDE-based electrode (Cu25; $L = 0.5 \text{ mgcm}^{-2}$) when applying a constant current of $j = 15 \text{ mA/cm}^2$. Besides C_2H_4 and CH_4 , CO and H_2 were also detected.

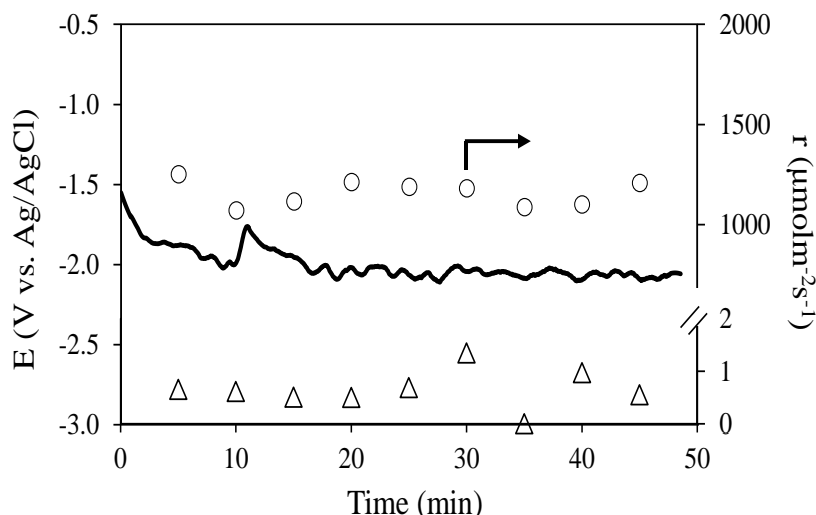


Figure 2. Time evolution for E and r in the production of C_2H_4 (circles) and CH_4 (triangles) at Cu25-based GDE. $j=15 \text{ mAcm}^{-2}$.

As shown in the figure, steady state conditions can be reached after 15 min of operation, when E remains constant (E averaged at -2.1 V vs. Ag/AgCl with a deviation of 5 %), although the fact that CO_2 is directly fed as gas to the cathodic compartment also provokes fluctuation in the voltage owing to the presence of bubbles. It is also worth noting that the evolution of E with time for the other materials (i.e. Cu40-60 and Cu60-80) shows a similar pseudo-stable behaviour after 15 min. The $r_{C_2H_4}$ and r_{CH_4} behave similarly, which may indicate the suitability of the Cu25-based electrode for the production of C_2H_4 and CH_4 after 45 min, even though material deactivation might occur at longer reaction times [21]. Future research efforts should include long-term stability test, which is essential to analyse the technical feasibility of the gas-phase CO_2 electroreduction process.

3.2.1. Particle size effect

Table 2 and figure 3 show the main results for the continuous gas-phase CO_2 reduction in the filter press electrochemical cell as a function of the Cu particle size.

Table 2. r and FE at Cu-based-GDEs as a function of the Cu NP size. $j=7.5 \text{ mAcm}^{-2}$.

Cu NP (nm)	E (V vs. Ag/AgCl)	r ($\mu\text{molm}^{-2}\text{s}^{-1}$)				S		FE (%)			
		H_2	CO	CH_4	C_2H_4	$S_{C_2H_4/CH_4}$	$S_{C_2H_4/H_2}$	H_2	CO	CH_4	C_2H_4
25	-1.7	366.6 ± 20	4.5 ± 1.3	37.6 ± 5.2	1148 ± 136	30.5	3.1	4.9	<0.1	2.0	92.8
40-60	-2.5	218.8 ± 7.0	16.7 ± 0.3	4.23 ± 0.5	216.7 ± 75	51.2	0.99	14.0	1.1	1.1	83.4
60-80	-2.2	184.7 ± 31	17.6 ± 1.8	4.1 ± 0.5	-	-	-	47.5	4.5	4.17	-

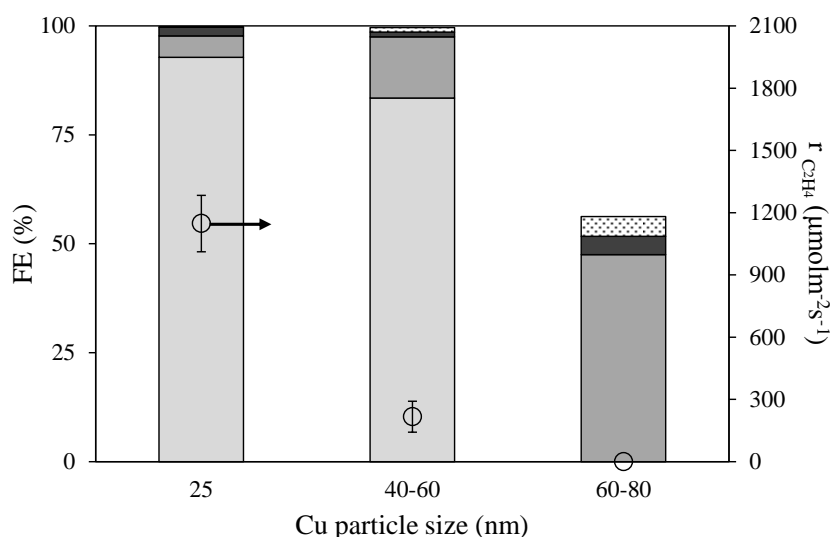


Figure 3. *FE* and $r_{C_2H_4}$ as a function of Cu NP size at $j=7.5 \text{ mAcm}^{-2}$. Colour codes for *FEs* (columns): light to dark shading (C_2H_4 , H_2 and CH_4 , respectively), and dotted points (CO).

From the results, a significant production of C_2H_4 was achieved at lower particle sizes. CH_4 , CO and H_2 were also observed over the entire Cu NP size range. In addition, lower rates for liquid-phase products such as CH_3OH ($r < 0.5 \mu\text{molm}^{-2}\text{s}^{-1}$) and C_2H_5OH ($r < 2.4 \mu\text{molm}^{-2}\text{s}^{-1}$) were detected with a *FE* $< 0.5 \%$. Previous findings in the group demonstrated that Cu60-80 are able to electroreduce CO_2 to CH_4 , also producing H_2 and CO in a wide range of applied potentials (i.e. from -2.4 V to -1.8 V vs. Ag/AgCl) and catalytic loadings (i.e. from 0.25 mgcm^{-2} to 1.5 mgcm^{-2}) in a MEA configuration [9]. The highest CH_4 production was achieved at 0.5 mgcm^{-2} and -2 V vs. Ag/AgCl ($j=7.5 \text{ mAcm}^{-2}$). However, C_2H_4 was not detected at this Cu NP size level (60-80 nm), in contrast to those results obtained in the present report when reducing particle size (i.e. Cu40-60 and Cu25). The absence of C_2H_4 at the largest Cu NP size tested (Cu60-80) may be associated with the lower presence of corners, specific crystal orientation surfaces, edges and defects in the electrocatalyst than those presented when reducing particle size [14, 27]. The presence of edge sites may represent key sites which facilitate the adsorption and stabilisation of CO_2 reduction reaction intermediates towards C-C coupling [28]. In contrast, the lower presence of these parameters at the largest particle size tested seems to be beneficial for CH_4 formation, at least in terms of *FE*. Consequently, it is crucial to identify which structural parameters in electrocatalysts for CO_2 electroreduction are able to control the selectivity of the reaction to multicarbon products.

The best values for C_2H_4 production were reached when using Cu25, in which a rate of $r=1148 \mu\text{molm}^{-2}\text{s}^{-1}$ and a *FE* of 92.8 % were obtained. In the same manner, the optimum CH_4 production rate was achieved at this particle size level ($r=37.6 \mu\text{molm}^{-2}\text{s}^{-1}$ with a *FE* of 2 %). This change in reaction performance compared to larger Cu NPs (i.e. 60-80 nm) also entails a decrease in the *FE* to H_2 and CO. In addition, the $S_{C_2H_4/H_2}$ was enhanced when decreasing the Cu particle size ($S_{C_2H_4/H_2}=3.1$ at Cu25) due to the presence of defects in the material in comparison to larger Cu particles ($S_{C_2H_4/H_2}=0.99$), whereas the highest $S_{C_2H_4/CH_4}$ was reached at Cu40-60 ($S_{C_2H_4/CH_4}=51.2$), in which CH_4 formation was considerably reduced in comparison to the Cu25 performance ($S_{C_2H_4/CH_4}=30.5$). Thus, the most active material for the reduction of CO_2 was Cu25, in agreement with the higher reduction response observed from CV profiles (figure 1). The literature shows that the formation of hydrocarbons from CO_2 can be suppressed at very small NPs (i.e. 2-15 nm) due to the reduction of catalytic active surface area as discussed by Reske et al. in 2014 [10], where the formation of syngas was preferred over the formation of

hydrocarbons. The authors suggested that very small (i.e. <3 nm) Cu catalysts should be avoided for the formation of hydrocarbons from CO₂ electroreduction

It is also worth noting that similar potentials are required to reach a current $j = 7.5 \text{ mAcm}^{-2}$ at Cu60-80 and Cu40-60 (-2.2 V vs. Ag/AgCl and -2.5 V vs. Ag/Cl, respectively). Nevertheless, a considerable decrease in the voltage needed is observed at Cu25 (-1.7 V vs. Ag/AgCl), which may involve lower energy consumptions to perform the CO₂ reduction reaction. These findings can be explained by alteration of energetic barriers for the different intermediates involved when decreasing Cu NP size, which may imply changes in product distribution (i.e. more reduced species can be obtained with higher rates).

3.2.2. Current density influence

Previous findings in our group demonstrated the possibility to modulate product yields with the applied current density [20, 29]. Thus, the performance of the system is evaluated at different current density levels in an attempt to enhance hydrocarbon yields. Table 3 and figure 4 summarised the productivity, selectivity and efficiency values at the Cu25-based GDEs as a function of the applied j .

Table 3. r and FE at Cu25-based-GDEs. $j = 7.5 - 30 \text{ mAcm}^{-2}$.

j (mAcm^{-2})	E (V vs. Ag/AgCl)	r ($\mu\text{molm}^{-2}\text{s}^{-1}$)				S		FE (%)			
		H ₂	CO	CH ₄	C ₂ H ₄	$S_{\text{C}_2\text{H}_4/\text{CH}_4}$	$S_{\text{C}_2\text{H}_4/\text{H}_2}$	H ₂	CO	CH ₄	C ₂ H ₄
7.5	-1.7	366.6 ± 20	4.5 ± 1.3	37.6 ± 5.2	1148 ± 136	30.5	3.1	4.9	<0.1	2.0	92.8
15	-2.1	682.4 ± 22	9.5 ± 7.3	4.8 ± 4.4	1242 ± 88	259	1.8	8.4	<0.15	0.2	91.2
30	-3.4	1034 ± 11	9.9 ± 8.0	5.5 ± 3.4	1165 ± 54	212	1.1	12.8	<0.15	0.3	86.8

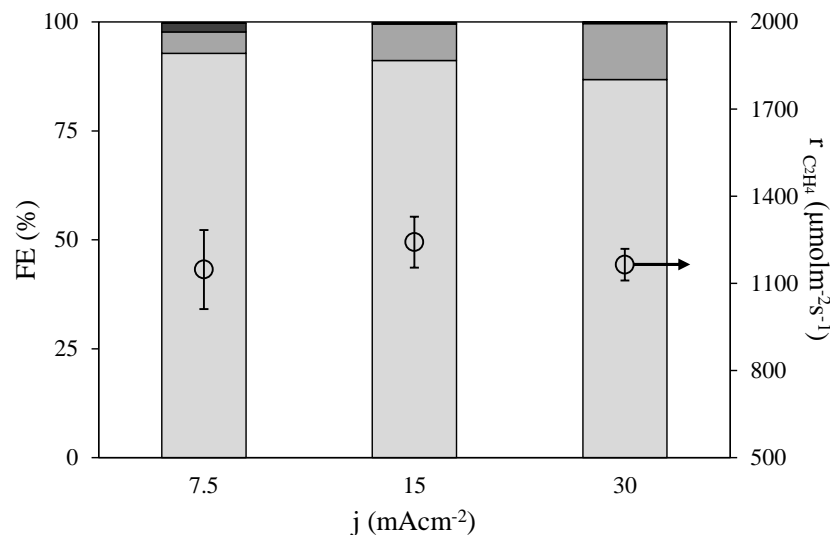


Figure 4. FE and $r_{\text{C}_2\text{H}_4}$ at different j on Cu25-based MEAs. Colour codes for FE s (columns): light to dark shading (C₂H₄, H₂ and CH₄, respectively).

As shown in table 3 and figure 4, the product distribution, rates and process efficiency are correlated with the current applied to the system. In this regard, the production of H₂ gained

importance when increasing j , involving a reduction in the FE to C_2H_4 (from 92.8% to 86.8%) and CH_4 (from 2.0 to 0.3), as well as in reaction selectivity ($S_{C_2H_4/H_2}$). This effect might be explained by the consumption of the additional current in producing H_2 (with only two electrons exchanged required) through the hydrogen evolution reaction instead of producing hydrocarbons from CO_2 electroreduction at higher j levels. Similarly, r to CH_4 is negatively affected by j , with $r=37.6 \mu\text{molm}^{-2}\text{s}^{-1}$ and $r=5.5 \mu\text{molm}^{-2}\text{s}^{-1}$ for $j=7.5 \text{ mAcm}^{-2}$ and $j=30 \text{ mAcm}^{-2}$, respectively. Additionally, the $S_{C_2H_4/CH_4}$ value goes from 30.5 to 212 when increasing the current from $j=7.5 \text{ mAcm}^{-2}$ to $j=30 \text{ mAcm}^{-2}$, respectively. On the other hand, CO (two electrons exchanged) productivity and efficiency were slightly improved at higher j probably because of the simplicity of the CO_2 -to- CO reaction (two electrons exchanged).

To sum up, applying a current density of $j=7.5 \text{ mAcm}^{-2}$, which allows achieving the highest C_2H_4 production ($r=1148 \mu\text{molm}^{-2}\text{s}^{-1}$, $FE=92.8$ and $S_{C_2H_4/H_2}=3.1$) with lower energy requirements ($E=-1.7 \text{ V}$ vs. $Ag/AgCl$), resulted in an improved gas-phase CO_2 electroreduction. This results may be taken into consideration when designing future applications for gas-phase CO_2 electroreduction processes.

3.2.3. Microporous layer evaluation

As discussed above, mass transfer limitations usually affect selectivity, productivity and efficiency in CO_2 electroreduction processes. Therefore, the use of a carbon MPL between the catalytic layer and the Toray carbon support may help to alleviate these limitations, favouring the transport of species (i.e. CO_2 and intermediates) in the filter-press cell. Table 4 shows the results for the presence/ absence of a MPL within the Cu25-based working electrode at the optimal current density level ($j=7.5 \text{ mAcm}^{-2}$).

Table 4. r and FE at Cu25 and MPL-Cu25-based-GDEs. $j=7.5 \text{ mAcm}^{-2}$.

MPL	E (V vs. $Ag/AgCl$)	r ($\mu\text{molm}^{-2}\text{s}^{-1}$)				S		FE (%)			
		H_2	CO	CH_4	C_2H_4	$S_{C_2H_4/CH_4}$	$S_{C_2H_4/H_2}$	H_2	CO	CH_4	C_2H_4
No	-1.7	366.6 ± 20	4.5 ± 1.3	37.6 ± 5.2	1148 ± 136	30.5	3.1	4.9	<0.1	2.0	92.8
Yes	-1.0	364.7 ± 22	5.6 ± 0.6	1.3 ± 0.4	816 ± 428	628	2.2	6.9	<0.15	<0.1	92.8

Similar C_2H_4 formation rates were obtained in the presence and absence of the MPL (considering experimental standard deviation). The same can be said for the FE to C_2H_4 . In the same manner, CO and H_2 production was not affected neither by the presence of an additional porous layer. Conversely, a decrease in CH_4 reaction rate (involving a significant increase in $S_{C_2H_4/CH_4}$) and FE was observed when using the MPL within the working electrode. The results may indicate that the presence of the MPL favoured the electrochemical reduction of CO_2 to more reduced products ($S_{C_2H_4/CH_4}=628$ vs. $S_{C_2H_4/CH_4}=30.5$ in its absence) with an insignificant effect on the C_2H_4/H_2 ratio. This finding can be probably associated to an improved transport of CO_2 through the working electrode.

Another advantage of the MPL seems to be the energy consumption, reaching voltage values of -1 V and -1.7 V vs. $Ag/AgCl$, for the presence and absence of the MPL, respectively. This can be justified by increases in the electrode conductivity, which is a key factor for an efficient CO_2 valorisation system.

287 Table 5 shows a summary of the r and FE to C_2H_4 and CH_4 (and other subproducts) from
 288 literature, paying attention to electrochemical reactor configuration (i.e. G: gas; L: liquid),
 289 electrocatalytic materials and process conditions.

290 **Table 5.** r and FE at CO_2 reduction systems with Cu-based electrodes.

Reactor type	Catalyst	E (V vs. Ag/AgCl)	FE (%)				r ($\mu\text{mol m}^{-2}\text{s}^{-1}$)		Other	Ref.
			H_2	CO	CH_4	C_2H_4	CH_4	C_2H_4		
G-L	Cu NP 25 nm	-1.7	4.9	<0.1	2.0	92.8	37.6	1148	CH_3OH , C_2H_5OH (traces)	This work
G-L	Cu-SPE ¹	-1.95	---	---	9.0	10.0	---	---	---	[24]
G-L	Cu gauze	-3.01	---	---	9.1	69	---	---	---	[30]
G-L	Cu-SPE ¹	-1.45	86.8	2.6	<0.1	8.8	---	---	HCOOH	[31]
G-L	Cu/C	---	79	0.3	4.5	---	---	---	HCOH, CH_3OH	[32]
G-L	Cu_2O/C	2.5 ²	45	---	30	5	---	---	CH_3OH	[33]
G-L	Cu_2O/C	2.5 ²	20	Low	10	---	0.005 ³	---	CH_3OH , C_2H_6	[34]
G-L	Cu/C	-1.8 ²	---	Low	Low	---	0.007	---	Alcohols	[26]
G-L	Cu/CNFs	---	---	---	---	---	0.001	---	CO , Alcohols, CH_3CHO	[35]
G-L	Cu NP	-2.0	41.5	3.22	4.5	---	4.4	---	---	[9]
L-L	Electropolished Cu	-1.65	20.5	1.3	33.3	25.5	---	---	Alcohols, HCOOH	[36]
L-L	Cu (110)	-1.75	18.8	---	49.5	15.1	---	---	Alcohols, HCOOH	[37]
L-L	Cu foil	-4.0	Low	17	60	15	---	---	HCOOH	[38]
L-L	Cu (100)	-1.6	6.8	0.9	30.4	40.4	---	---	HCOOH	[12]
L-L	CuBr-Cu mesh	-2.4	9.3	2.4	5.8	79.5	---	---	C_2H_6	[39]
L-L	Cu foil	-3.0	17.9	3.2	70.5	3.1	---	---	HCOOH	[40]
L-L	Polished Cu	-1.9	40	7	19.4	18.7	---	---	---	[41]
L-L	Cu foil	-1.35	52	<2 %	40	10	---	---	HCOOH, alcohols, CH_3CHO	[42]
L-L	Cu NP	-1.3	28	33	2	35	---	---	C_2H_6	[43]
L-L	Cu mesh	-1.9	Balance	5	15	8	---	---	---	[44]
L-L	Polypyrrole coated Cu	-3 V ⁴	Not analysed	15.1	25.5	3.1	---	---	HCOOH, CH_3COOH	[45]
L-L	Cu layers on Pt	-1.2	Balance	---	33	7	---	---	---	[46]
L-L	Cu foil	-1.35	45	---	30	---	---	---	---	[47]

L-L	Electrode posited Cu NP	-2.2	5	2.5	60	20	---	---	---	[14]
L-L	Cu foil	-1.3	20	3	57	20	---	---	---	[10]
L-L	Cu nanoneed les	-1.4	18	---	14	6	---	---	HCOOH	[48]
L-L	Cu nanofoa m	-1.7	60	7.5	0.2	1.3	---	---	HCOOH, C ₂ H ₆	[49]
L-L	Cu NP	-1.55	25	---	76	---	---	---	---	[50]
L-L	Deposite d Cu ₂ O	-1.3	Balance	3	5	37.5	---	---	C ₂ H ₆	[51]
L-L	Cu ₂ O over Cu	-1.19	39	Low	Low	39	---	---	HCOOH, C ₂ H ₆ , C ₂ H ₅ OH	[52]
L-L	Cu ₂ O- derived Cu	-1.2	18	Low	Low	Low	---	---	HCOOH, C ₂ H ₆ (30 %), C ₂ H ₅ OH,	[53]
L-L	Cu mesocrys tals	-1.19	60	2	2.7	27.2	---	---	HCOOH	[54]
L-L	Cu ₂ O reduced to Cu	-1.8	24	Low	2	44	---	---	---	[27]
L-L	Electrode posited Cu	-1.4	30	---	28	---	---	---	C ₂ H ₆ (43 %)	[55]
L-L	Cu foil	-1.6	15	1	70	15	62	5	---	[56]
L-L	Oxide- derived Cu	-1.0	15	15	---	20	---	250 ⁵	HCOOH, C ₂ H ₆ (35 %)	[57]
L-L	Cu foil	-1.2	15	1	60	20	10	6	HCOOH	[58]
L-L	Cu foil+glyc ine	-1.9	---	---	30	25	---	---	C ₂ H ₆ , C ₃ H ₈	[59]
L-L	Cu + graphene oxide	-1.5	50	Low	40	Low	---	---	HCOOH	[60]
L-L	Cu foil	-1.65	---	---	45	2	---	---	HCOOH	[61]
L-L	Cu ₂ O- CuBr films	-2.1	81	---	---	17	---	---	C ₂ H ₆	[62]
L-L ⁶	Cu sheet	-1.6	30	Low	10	30	250 ⁷	140 ⁷	---	[63]
L-L	Cu mesh	-1.9	---	5	10	37	---	---	---	[13]
L-L	Cu films	-1.6	21	5	4	40	---	---	---	[64]
G-G	Cu deposit	---	---	---	0.11	1.7	---	---	C ₂ H ₆	[65]
G-G	Cu felt	3.9 ²	---	---	0.12	---	---	---	Long- chain Hydrocarb	[66]

Notation: ¹solid polymer electrolyte, ²unknown reference electrode, ³ $\mu\text{mol s}^{-1}$, ⁴Pb(Hg)x/PbSO₄/SO₄²⁻ reference electrode, ⁵ppm $\text{cm}^{-2}\text{h}^{-1}$, ⁶CO₂ (70 %)- O₂ (30 %) inlet, ⁷ppm.

As observed, this work reports the highest productivity values for C₂H₄ ($r_{\text{C}_2\text{H}_4}=1148 \mu\text{mol m}^{-2}\text{s}^{-1}$) and one of the highest for CH₄ ($r_{\text{CH}_4}=37.6 \mu\text{mol m}^{-2}\text{s}^{-1}$) achieved so far, which denotes the relevance of the work. Besides, the highest *FE* to C₂H₄ has been also reached with this study (92.8 %) at Cu25-based GDEs. However, higher *FEs* to CH₄ have been reported in literature for G-L and L-L systems (up to 76 %). It is also worth noting that several researchers have detected long-chain hydrocarbons at different Cu-based catalytic material (i.e. electrodeposited Cu, oxide-derived Cu, Cu+glycine, etc.), with higher *FEs* to C₂H₆ (e.g. 43 %). In any case, most of the systems are more selective to H₂, which should be reduced if we intend to increase the formation of hydrocarbons.

To sum up, further advances are needed to improve the key parameters for the electroreduction of CO₂ to hydrocarbons (i.e. *r*, *S*, *FE*, energy consumption, etc.) in order to get closer to real applications. The authors recommend focusing future research on the development of alternative catalytic materials (i), reactor configurations (ii) and ion-exchange membranes (iii). Additionally, a deeper understanding on reaction mechanisms (iv) is required to better understand the behaviour of the system.

i) Alternative catalytic materials. Highly active electrocatalysts should be developed in order to boost *r* and *FEs* to hydrocarbons. In this regard, particle size, crystal orientation and catalyst shapes need to be controlled, owing to their influence on the selectivity of the electrochemical reaction. In addition, the combination of other metals with Cu (i.e. multimetallic electrocatalysts) may imply changes in reaction pathways and intermediates, involving a reduction of the overpotential and the competitive hydrogen evolution reaction. The application of new catalyst structures, such as metal organic frameworks (MOFs) may be also interesting due to their tunable structure.

ii) Reactor configurations. Electrochemical reactors have an essential role in the progress of CO₂-valorisation processes because of mass transfer limitations, which limits the widespread use of the technology. CO₂ solubility issues should also be taken into account. These limitations may be overcome by the application of GDEs and MEAs. Therefore, the possibility of suppressing the liquid phase from the electrochemical systems (i.e. G-L and G-G configurations) are attractive, even though big efforts are still required to make progresses in this field.

iii) Ion-exchange membranes. Highly conductive cation exchange membranes are needed to carry out the electrochemical CO₂ reduction to hydrocarbons because of the high number of protons involved in the reaction. Therefore, the development of alternative conductive membrane materials is required in order to replace the costly Nafion membranes.

iv) Mechanisms understanding. The key determining step in CO₂ reduction seems to be the protonation of adsorbed CO to obtain CHO. On the one hand, the pathway for the formation of CH₄ at Cu surfaces involves further protonation steps of adsorbed CHO, in which OCH₃ adsorbed is finally protonated to produce CH₄, with different intermediates involved depending on crystal orientation and lattice, among others. On the other hand, the formation of C₂H₄ requires C-C bonding and adsorbed CH₂O species seems to be key intermediates for further dimerization to obtain C₂H₄. In any case, the reaction pathway is still unclear and further research efforts are required in this regard.

4. Conclusions

This work presents innovative results on the continuous production of hydrocarbons (i.e. ethylene and methane) from gas-phase CO₂ electroreduction at Cu-based electrodes including different nanoparticles sizes (ranging from 25 nm to 80 nm). Cyclic voltammetry tests showed that Cu 25 nm-based electrodes displayed an improved performance in comparison to larger Cu particles (i.e. 40-60 nm and 60-80 nm), which can be explained by an increase in the fraction of under-coordinated sites when decreasing particle size.

The highest ethylene production (1148 $\mu\text{mol m}^{-2}\text{s}^{-1}$) was achieved at the lowest particle size level tested (i.e. 25 nm), with a Faraday efficiency of 92.8 %. When increasing Cu particle size (i.e. 40-60 nm and 60-80 nm) the productivity and the Faraday efficiency to C₂H₄ was negatively affected, involving also higher overpotentials. Conversely, ethylene/methane ratio was enhanced at the 40-60 nm-based electrodes (50.4), although the hydrogen evolution is also improved (ethylene/hydrogen= 0.99) compared to those obtained at the lowest particle size level (3.1). In addition, similar ethylene rates were achieved in the whole current density range (7.5 mAcm⁻² to 30 mAcm⁻²), while the Faraday efficiency to ethylene decreased. Finally, the use of a microporous layer led to higher ethylene/methane ratios with an insignificant effect on ethylene/hydrogen ratios, which means that the presence of the MPL favours the electrochemical reduction of CO₂ to more reduced products.

Overall, the productivity, selectivity and efficiency of the gas-phase CO₂ electroreduction to hydrocarbons are highly dependent on the Cu particle size. Other aspects such as crystal orientation and shape, among others, should be considered in future research for an efficient CO₂ electroreduction to hydrocarbons process.

Acknowledgements

The authors gratefully acknowledge the financial support from the Spanish Ministry of Economy and Competitiveness (MINECO) through the projects CTQ2013-48280-C3-1-R and CTQ2016-76231-C2-1-R. Ivan Merino-Garcia and Jonathan Albo would also like to thank the MINECO for the Early Stage Researcher Contract (BES2014-070081) and Ramón y Cajal programme (RYC-2015-17080), respectively.

References

- [1] National Oceanic and Atmospheric Administration (NOAA), *Carbon dioxide levels rose at record pace for 2nd straight year*, March 10th, 2017. Available on: <http://www.noaa.gov/news/carbon-dioxide-levels-rose-at-record-pace-for-2nd-straight-year>
- [2] Albo J, Alvarez-Guerra M, Castaño P and Irabien A 2015 *Green Chem.* **17** 2304
- [3] Kondratenko E V, Mul G, Baltrusaitis J, Larrazabal G O and Perez-Ramirez J 2013 *Energy Environ. Sci.* **6** 3112
- [4] Jhong H R M, Ma S and Kenis P J A 2013 *Curr. Opin. Chem. Eng.* **2** 191
- [5] Qiao J, Liu Y, Hong F and Zhang J 2014 *Chem. Soc. Rev.* **43** 631
- [6] Martín A J, Larrazábal G O and Pérez-Ramírez J 2015 *Green Chem.* **17** 5114
- [7] Wu J and Zhou X-D 2016 *Chin. J. Catal.* **37** 999
- [8] Durand W J, Peterson A A, Studt F, Abild-Pedersen F and Nørskov J K 2011 *Surf. Sci.* **605** 1354
- [9] Merino-Garcia I, Albo J and Irabien A 2017 *Energy Technol.* **5** 922

379 [10] Reske R, Mistry H, Behafarid F, Cuenya B R and Strasser P 2014 *J. Am. Chem. Soc.* **136**
380 6978

381 [11] Hori Y, Takahashi I, Koga O and Hoshi N 2002 *J. Phys. Chem. B* **106** 15

382 [12] Hori Y, Takahashi I, Koga O, Hoshi N 2003 *J. Mol. Catal. A: Chem.* **199** 39

383 [13] Yang K D, Ko W R, Lee J H, Kim S J, Lee H, Lee M H and Nam K T 2017 *Angew. Chem.*
384 *Int. Ed.* **56** 796

385 [14] Baturina O A *et al.* 2014 *ACS Catal.* **4** 3682

386 [15] Corradini P G, Pires F I, Paganin V A, Perez J and Antolini E 2012 *J. Nanopart. Res.* **14**
387 1080

388 [16] Jaramillo T F, Baeck S-H, Cuenya B R and McFarland E W 2003 *J. Am. Chem. Soc.* **125**
389 7148

390 [17] Merino-Garcia I, Alvarez-Guerra E, Albo J and Irabien A 2016 *Chem. Eng. J.* **305** 104

391 [18] Endrődi B, Bencsik G, Darvas F, Jones R, Rajeshwar K and Janáky C 2017 *Prog. Energy*
392 *Combust. Sci.* **62** 133.

393 [19] Delacourt C, Ridgway P L, Kerr and Newman J 2008 *J. Electrochem. Soc.* **155** B42

394 [20] Del Castillo A, Alvarez-Guerra M, Solla-Gullón J, Sáez A, Montiel V and Irabien A 2017
395 *J. CO2 Util.* **18** 222

396 [21] Albo J and Irabien A 2016 *J. Catal.* **343** 232

397 [22] Salehi-Khojin A, Jhong H R M, Rosen B A, Zhu W, Ma S, Kenis P J A and Masel R I 2013
398 *J. Phys. Chem. C* **117** 1627

399 [23] Ampelli C, Genovese C, Errahali M, Gatti G, Marchese L, Perathoner S and Centi G 2015
400 *J. Appl. Electrochem.* **45** 701

401 [24] Dewulf D W and Bard A J 1988 *Catal. Lett.* **1** 73

402 [25] Jiménez C, García J, Camarillo R, Martínez F and Rincón J 2017 *Energy Fuels* **31** 3038

403 [26] Gutiérrez-Guerra N, Moreno-López L, Serrano-Ruiz J C, Valverde J L and de Lucas-
404 Consuegra A 2016 *Appl. Catal. B* **188** 272

405 [27] Kas R, Kortlever R, Yilmaz H, Koper M T M and Mul G 2015 *ChemElectroChem* **2** 354

406 [28] Loiudice A, Lobaccaro P, Kamali E A, Thao T, Huang B H, Ager J W and Buonsanti R
407 2016 *Angew. Chem. Int. Ed.* **55** 5789

408 [29] Albo J, Vallejo D, Beobide G, Castillo O, Castaño P and Irabien A 2017 *ChemSusChem* **10**
409 1100

410 [30] Cook R L, Macduff R C and Sammells A F 1990 *J. Electrochem. Soc.* **137** 607

411 [31] Komatsu S, Tanaka M, Okumura A and Kungi A 1995 *Electrochim. Acta* **40** 745

412 [32] Aeshala L M, Rahman S U and Verma A 2012 *Sep. Purif. Technol.* **94** 131

413 [33] Aeshala L M, Uppaluri R and Verma A 2013 *J. CO2 Util.* **3-4** 49

414 [34] Aeshala L M, Uppaluri R and Verma A 2014 *Phys. Chem. Chem. Phys.* **16** 17588

415 [35] Gutiérrez-Guerra N, Valverde J L, Romero A, Serrano-Ruiz J C and de Lucas-Consuegra A
416 2017 *Electrochem. Commun.* **81** 128

417 [36] Hori Y, Wakebe H, Tsukamoto T and Koga O 1994 *Electrochim. Acta* **39**, 1833

418 [37] Hori Y, Wakebe H, Tsukamoto T and Koga O 1995 *Surf. Sci.* **335** 258

419 [38] Kaneco S, Iiba K, Suzuki S K, Ohta K and Mizuno T 1999 *J. Phys. Chem. B* **103** 7456

420 [39] Yano H, Tanaka T, Nakayama M and Ogura K 2004 *J. Electroanal. Chem.* **565** 287

421 [40] Kaneco S, Katsumata H, Suzuki T and Ohta K 2006 *Energy Fuels* **20** 409

422 [41] Gonçalves M R, Gomes A, Condeço J, Fernandes R, Pardal T, Sequeira C A C and Branco
423 J B 2010 *Energy Convers. Manage.* **51** 30

424 [42] Kuhl K P, Cave E R, Abram D N and Jaramillo T F 2012 *Energy Environ. Sci.* **5** 7050

425 [43] Tang W, Peterson A A, Varela A S, Jovanov Z P, Bech L, Durand W J, Dahl S, Nørskov J
426 K and Chorkendorff I 2012 *Phys. Chem. Chem. Phys.* **14**, 76

427 [44] Gonçalves M R, Gomes A, Condeço J, Fernandes R, Pardal T, Sequeira C A C and Branco
428 J B 2013 *Electrochim. Acta* **102** 388

429 [45] Aydin R, Dogan H O and Köleli F 2013 *Appl. Catal. B* **140-141** 478

430 [46] Reske R, Duca M, Oezaslan M, Schouten K J P, Koper M T M and Strasser P 2013 *J.*
431 *Phys. Chem. Lett.* **4** 2410

432 [47] Varela A S, Schlaup C, Jovanov Z P, Malacrida P, Horch S, Stephens I E L and
433 Chorkendorff I 2013 *J. Phys. Chem. C* **117** 20500

434 [48] Xie J, Huang Y and Yu H 2015 *Front. Environ. Sci. Eng.* **9** 861

435 [49] Sen S, Liu D, Tayhas G and Palmore R 2014 *ACS Catal.* **4** 3091

436 [50] Manthiram K, Beberwyck B J and Alivisatos A P 2014 *J. Am. Chem. Soc.* **136** 13319

437 [51] Kas R, Kortlever R, Milbrat A, Koper M T M, Mul G and Baltrusaitis J 2014 *Phys. Chem.*
438 *Chem. Phys.* **16** 12194

439 [52] Ren D, Deng Y, Handoko A D, Chen C S, Malkhandi S and Yeo B S 2015 *ACS Catal.* **5**
440 2814

441 [53] Chen C S, Wan J H and Yeo B S 2015 *J. Phys. Chem. C* **119** 26875

442 [54] Chen C S, Handoko A D, Wan J H, Ma L, Ren D and Yeo B S 2015 *Catal. Sci. Technol.* **5**
443 161

444 [55] Keerthiga G, Viswanathan B and Chetty R 2015 *Catal. Today* **245** 68

445 [56] Varela A S, Kroschel M, Reier T and Strasser P 2016 *Catal. Today* **260** 8

446 [57] Dutta A, Rahaman M, Luedi N C, Mohos M and Broekmann P 2016 *ACS Catal.* **6** 3804

447 [58] Varela A S, Ju W, Reier T and Strasser P 2016 *ACS Catal.* **6** 2136

448 [59] Xie M S, Xia B Y, Li W, Yan Y, Yang, Y, Sun Q, Chan S H, Fisher A and Wang X 2016
449 *Energy Environ. Sci.* **9** 1687

450 [60] Lum Y, Kwon Y, Lobaccaro P, Chen L, Clark E L, Bell A T and Ager J W 2016 *ACS*
451 *Catal.* **6** 202

452 [61] Bevilacqua M, Filippi J, Folliero M, Lavacchi A, Miller H A, Marchionni A and Vizza F
453 2016 *Energy Technol.* **4** 1020

454 [62] De Tacconi N R, Chanmanee W, Dennis B H and Rajeshwar K 2017 *J. Mater. Res.* **32**
455 1727

456 [63] Engelbrecht A, Hämmerle M, Moos R and Fleischer M 2017 *Electrochim. Acta* **224** 642

457 [64] Padilla M, Baturina O, Gordon J P, Artyushkova K, Atanassov P and Serov A 2017 *J. CO2*
458 *Util.* **19** 137

459 [65] Cook R L, MacDuff R C and Sammells F 1988 *J. Electrochem. Soc.* **135** 1470

460 [66] Kriescher S M A, Kugler K, Hosseiny S S, Gendel Y and Wessling M 2015 *Electrochem.*
461 *Commun.* **50** 64